13th International Conference on
Structural Health Monitoring of Intelligent Infrastructure
DOI: 10.3217/978-3-99161-057-1-110

Etched fiber Bragg grating sensor-based groundwater salinity monitoring for seawater intrusion

Hongtao Jiang[1], Junyi Guo[2], Bin Shi[2], Mengya Sun[3], Guangqing Wei[4]
[1] School of Geographic and Oceanographic Science, Nanjing University, No.163 Xianlin Avenue, 210023 Nanjing, China
[2] School of Earth Sciences and Engineering, Nanjing University, No.163 Xianlin Avenue, 210023 Nanjing, China
[3] School of Earth Sciences and Engineering, Hohai University, No. 8 Focheng West Road, 210098 Nanjing, China
[4] Suzhou Nanzee Sensing Technology Co., Ltd, No.150 Renai Avenue, 215123 Suzhou, China

email: jianghongtao@nju.edu.cn, gjy@smail.nju.edu.cn, shibin@nju.edu.cn, smy@hhu.edu.cn, wgq@nzsensing.com

ABSTRACT: As global climate change drives rising sea levels, coastal regions face growing threats from seawater intrusion. This process increases groundwater salinity, accelerating steel corrosion and compromising the structural integrity of concrete infrastructure. However, addressing these challenges is limited by existing salinity monitoring technologies, which often suffer from slow response times and low sensitivity in in-situ conditions. This study proposes a salinity sensor based on Fiber Bragg Grating (FBG), enhanced by chemically etching the fiber cladding to create an etched FBG (EFBG). This modification improves sensitivity to external refractive indices for accurate salinity detection. A three-layer waveguide dispersion model simulated wavelength shifts during sensor etching and testing using MATLAB, revealing how etching diameters impact sensitivity and confirming a linear relationship between wavelength and seawater salinity. To improve EFBG durability and reduce hydrofluoric acid damage, the etching process was divided into rapid, stable, and fine stages. Results demonstrated that higher etching levels increased sensitivity, achieving a sensitivity coefficient of up to 29.432 pm/% in specific conditions. The EFBG salinity sensor offers high sensitivity, fast response, compact size, corrosion resistance, and interference immunity, making it ideal for in-situ groundwater salinity monitoring in aquifers and mitigating risks to coastal structural health.

KEY WORDS: Salinity; Fiber Bragg grating (FBG); Chemical etching; Seawater Intrusion.

1 INTROFUCTION

Excessive groundwater extraction in coastal areas disrupts the natural balance between freshwater and seawater, driving inland migration of the saltwater-freshwater interface — a phenomenon known as seawater intrusion [1,2]. This process significantly increases groundwater salinity, which accelerates corrosion of steel reinforcements and compromises the structural integrity of concrete infrastructure in coastal regions, posing severe risks to long-term structural health and safety [3].

Monitoring groundwater salinity is crucial for assessing seawater intrusion severity and protecting infrastructure [4,5]. Existing monitoring techniques include electrical conductivity sensors, microwave remote sensing, and fiber optic sensors. Electrical conductivity sensors offer high accuracy, but inductive types are vulnerable to electromagnetic interference, while electrode types suffer from fouling, limiting long-term performance[6,7]. Microwave remote sensing enables large-scale surface salinity observation, but it cannot penetrate below the surface or provide in-situ groundwater monitoring [8,9].

Fiber optic sensors have attracted increasing attention due to their compact size, immunity to electromagnetic interference, and high sensitivity [10]. Among them, Fiber Bragg Grating (FBG)-based salinity sensors can be divided into polymer-coated FBGs and etched FBGs (EFBGs). Polymer-coated sensors, such as those developed by Jun Cong et al. (2002) [11] and Ping Lu et al. (2008) [12], achieve moderate sensitivity, but suffer from slow response and poor repeatability due to polymer swelling and hysteresis.

To improve sensitivity, Kerstin Schroeder et al. (2001) [13] introduced a side-polished FBG, exposing the evanescent field for salinity detection, but the sensor exhibited non-linear response in varying temperature and salinity environments. Pereira et al. (2004) [14] used hydrofluoric acid to etch FBGs, achieving a salinity sensitivity of 1.28 pm/%, but this approach lacked robust in-situ adaptation for groundwater monitoring.

Most existing EFBG sensors focus on biochemical sensing, with limited research targeting long-term groundwater salinity monitoring for seawater intrusion detection. This study develops a high-sensitivity, fast-response EFBG salinity sensor capable of salinity measurement, providing a compact and reliable solution for real-time in-situ groundwater salinity monitoring, contributing to the protection of coastal groundwater resources and infrastructure health.

2 FUNDAMENTAL PRINCIPLE OF EFBG FOR SEAWATER SALINITY SENSING

A Fiber Bragg Grating (FBG) is a reflective grating structure inscribed in the core of an optical fiber. When broadband light propagates along the fiber axis, the FBG reflects a specific wavelength, known as the Bragg wavelength, which is determined by the effective refractive index of the fiber core and the grating period, as shown in Figure 1 [15].

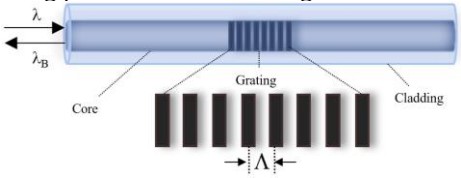

Figure 1. The schematic diagram of FBG sensing principle.

The Bragg wavelength λ_B satisfies the following relationship [16]:

$$\lambda_B = 2n_{eff}\Lambda \quad (1)$$

DOI: 10.3217/978-3-99161-057-1-110

where n_{eff} denotes the effective refractive index of the fiber core, and Λ represents the grating period.

In conventional optical fibers, the presence of a complete cladding layer confines light within the fiber core, making the Bragg wavelength largely insensitive to changes in the external refractive index. However, by physically or chemically reducing the cladding thickness, a portion of the light propagating in the core extends into the surrounding medium as an evanescent field. This modification allows the effective refractive index n_{eff} to be influenced by the external refractive index, thereby shifting the Bragg wavelength λ_B.

As the cladding thickness decreases, the optical fiber gradually forms a three-layer waveguide structure, consisting of the external medium, the remaining cladding, and the core. The modal characteristics of light propagation change accordingly, and the propagation constant β is also affected. To quantify the influence of cladding etching on the propagation constant, the corrected propagation constant for different etched diameters can be expressed as [17]:

$$\beta = \beta_0 + \kappa\eta_P(n_{SRI} - n_{cl}) \tag{2}$$

where β_0 represents the propagation constant under normal conditions, k denotes the wave vector, and α is the power loss coefficient, representing the proportion of power loss in the etched region relative to the total guided power. n_{ext} and n_{clad} denote the refractive indices of the external medium and the cladding, respectively.

From the definition of the propagation constant, the effective refractive index n_{eff} can be derived as:

$$\partial n_{eff} = \partial n \partial \eta \tag{3}$$

At the end of the etching process, the effective refractive index reaches a stable value, denoted as $n_{eff,\,final}$. Combining this with Equations (1), (2), and (3), the relationship between Bragg wavelength shift and external refractive index can be obtained:

$$\partial\lambda_B = 2\Lambda\eta_0(n_{SRI} - n_{cl}) \tag{4}$$

This indicates that after etching to a certain diameter, the Bragg wavelength becomes highly sensitive to changes in the external refractive index.

In practice, the primary salt component in seawater is sodium chloride (NaCl). Therefore, the salinity of seawater can be approximated using NaCl solution concentration. At constant temperature, the refractive index of NaCl solution exhibits a linear relationship with salinity [18]:

$$c(\%) = k_s n_{SRI} - k_0 \tag{5}$$

where k_s is the salinity coefficient, which remains constant under fixed external conditions when only salinity changes. In this study, k_s is set to 540.5405, and k_0 is 720.5946.

3 NUMERICAL MODEL FOR EFBG SEAWATER SALINITY SENSING

To further establish the quantitative relationship between EFBG wavelength shifts and seawater salinity, a numerical analysis was conducted using MATLAB. The calculation of the effective refractive index requires a fiber waveguide model, which can be divided into two-layer and three-layer structures, as shown in Figure 2.

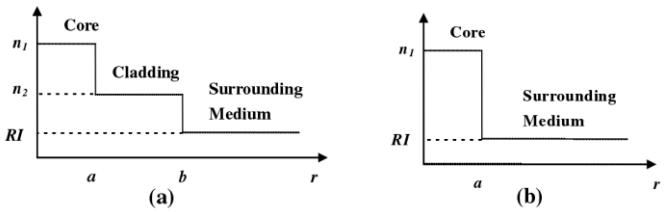

Figure 2. Two types of fiber waveguide models: (a) Three-layer structure; (b) Two-layer structure.

When the fiber cladding is fully etched away or the etching extends into the fiber core, the core and external medium form a simple two-layer circular waveguide model (Figure 2(a)). This type, known as the core-etched FBG, offers high salinity sensitivity. However, due to severe cladding removal, the mechanical strength is significantly reduced, resulting in poor robustness, which limits its suitability for long-term monitoring in harsh environments. To balance mechanical integrity and sensitivity, this study employs a partially etched FBG structure, modeled as a three-layer circular waveguide (Figure 2(b)). The dispersion equation for the three-layer fiber waveguide can be expressed as follows [19]:

$$\begin{cases} \dfrac{[\hat{J}_m(u)-\hat{Y}_m(u'c)][\hat{K}_m(v)-\hat{J}_m(u')]}{[\hat{J}_m(u)-\hat{J}_m(u'c)][\hat{K}_m(v)-\hat{Y}_m(u')]} = \dfrac{J_{m+1}(u'c)Y_{m+1}(u')}{J_{m+1}(u')Y_{m+1}(u'c)} & (\beta < k_0 n_{cl}) \\ \dfrac{[\hat{J}_m(u)-\hat{K}_m(v'c)][\hat{K}_m(v)+\hat{I}_m(v')]}{[\hat{J}_m(u)+\hat{I}_m(v'c)][\hat{K}_m(v)-\hat{K}_m(v')]} = \dfrac{I_{m+1}(v'c)K_{m+1}(v')}{I_{m+1}(v')K_{m+1}(v'c)} & ((\beta > k_0 n_{cl}) \end{cases} \tag{6}$$

The mathematical symbols and parameters used in the equation are defined as:

$$\widehat{Z_m}(x) = \frac{Z_m(x)}{xZ_{m+1}(x)} \tag{7}$$

$$u = a_1(k_0^2 n_1^2 - \beta^2)^{1/2} \tag{8}$$

$$u' = a_2(k_0^2 n_{cl}^2 - \beta^2)^{1/2} \tag{9}$$

$$v' = a_2(\beta^2 - k_0^2 n_{cl}^2)^{1/2} \tag{10}$$

$$v = a_2(\beta^2 - k_0^2 n_{SRI}^2)^{1/2} \tag{11}$$

$$c = \frac{a_1}{a_2} \tag{12}$$

where k_0 denotes the vacuum wave number. The fiber parameters used in this model match the experimental optical fiber specifications discussed later. J_m and Y_m represent the first and second kind Bessel functions, respectively, while I_m and K_m denote the modified first and second kind Bessel functions.

Based on the above equations, MATLAB was used to calculate the relationship between FBG wavelength and fiber diameter during the etching process. Figure 3 illustrates the variation in Bragg wavelength as a function of fiber diameter when the external refractive index is set to 1.333.

DOI: 10.3217/978-3-99161-057-1-110

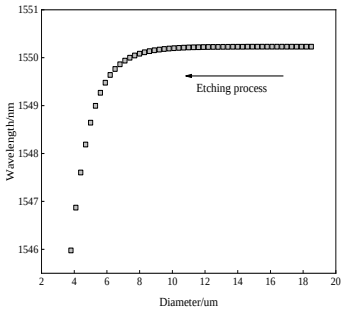

Figure 3 Diagram of wavelength variation as a function of diameter during etching.

As shown in Figure 3, at the initial stage of etching, the thick cladding confines the optical field within the core, making the wavelength almost insensitive to the external refractive index. As etching progresses and the cladding becomes thinner, the evanescent field begins to interact with the external environment. Due to the lower refractive index of the surrounding medium compared to the cladding, the Bragg wavelength decreases sharply as the diameter decreases. This trend provides a basis for real-time monitoring of fiber diameter during the etching process.

The surface salinity of seawater typically ranges from 3.4% to 3.7%. To evaluate the feasibility of EFBG sensors for seawater salinity monitoring, MATLAB simulations were carried out to investigate the relationship between salinity and wavelength shift under low-salinity conditions. As shown in Figure 4, the smaller the fiber diameter, the higher the salinity sensitivity. Within the salinity range of 0–6%, EFBG sensors with different diameters all exhibit a clear linear relationship between salinity and wavelength shift. Higher etching levels consistently lead to increased salinity sensitivity, providing important design and fabrication guidelines for EFBG-based salinity sensors.

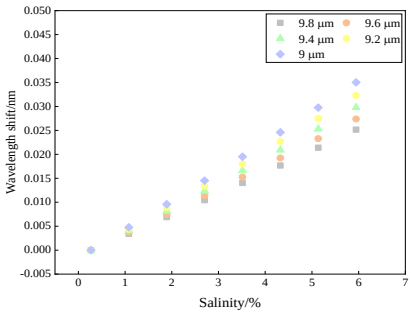

Figure 4 Relationship between wavelength variation and salinity at low salinity.

4 EXPERIMENTAL DESIGN AND SALINITY SENSING TESTS

4.1 Etching Process

The fiber optic sensing element used in this study is a single-point fiber Bragg grating sensor with a central wavelength of 1564 nm, a wavelength tolerance of ±0.2 nm, and a grating length of 10 mm. The fiber is coated with an acrylate layer, with a reflectivity of 88.3%, a 3 dB bandwidth of 0.23 nm, and a side mode suppression ratio of 22 dB. The core diameter is 9 μm, cladding diameter is 125 μm, and the coating diameter is 240 μm, consistent with the parameters used in the numerical simulations.

Hydrofluoric acid (HF), known for its strong corrosive properties on glass and silicon-based materials, was used to etch the fiber cladding. The initial HF concentration was 40%, which was diluted with distilled water to prepare solutions of lower concentrations for staged etching. During the etching process, the non-grating sections of the fiber were covered with paraffin wax to protect them from unnecessary etching. The fiber was also connected to an NZS-FBG-A01 interrogator (*Suzhou Nanzhi Sensing Technology Co., Ltd.*) via patch cords to monitor real-time Bragg wavelength shifts, allowing precise control over the final cladding diameter. The interrogator operates in the wavelength range of 1528-1568 nm with a resolution of 1 pm. To ensure the reliability of etching rate measurements, three bare fibers were fixed in parallel on a T-shaped plastic holder and immersed in HF solutions for parallel etching experiments. Each etching session lasted 60 minutes, after which the fibers were thoroughly rinsed with deionized water to remove residual acid and air-dried in a ventilated area. The diameters of the fibers were measured under an optical microscope, and the average diameter of the three fibers was recorded for each condition. This process was repeated to determine etching rates at different HF concentrations.

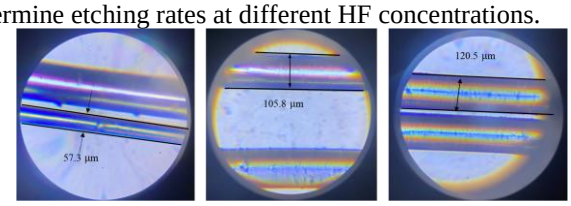

Figure 5. Microscope images of bare fibers etched by hydrofluoric acid at different concentrations: (a) 40% concentration; (b) 20% concentration; (c) 5.7% concentration.

The results show that higher HF concentrations lead to faster etching rates but also create rougher fiber surfaces, as shown in Figure 5. To reduce surface irregularities, minimize residual stress, and improve the wavelength stability of the sensor, a staged etching process was employed. In this process, high-concentration HF was first used for rapid bulk etching, followed by lower-concentration HF for gradual surface refinement. This method ensures a smoother grating surface and reduces unwanted stress-induced wavelength shifts.

4.2 Salinity Testing

To simulate coastal groundwater conditions, artificial seawater with salinities ranging from 0% to 6% (in 1% increments) was prepared by dissolving NaCl in distilled water. The EFBG sensor was sequentially immersed in these solutions, and the Bragg wavelength was recorded in real time to evaluate its response to salinity changes.

DOI: 10.3217/978-3-99161-057-1-110

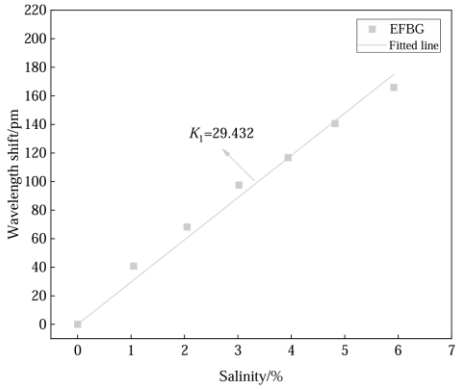

Figure 6. Bragg wavelength variation at different salinities.

The initial wavelength offset of the EFBG was 7.5 nm. Based on the diameter-wavelength relationship established through numerical analysis, the cladding diameter of the EFBG was calculated to be 14.82 μm. The measured Bragg wavelength shifts at different salinity levels are shown in Figure 6. As illustrated, the Bragg wavelength shift increases significantly with rising salinity and demonstrates a clear linear relationship with salinity. The EFBG sensor achieved a salinity sensitivity of 29.432 pm/%, confirming its potential for high-sensitivity salinity monitoring.

5 CONCLUSION

This study developed an etched fiber Bragg grating (EFBG) sensor for in-situ monitoring of groundwater salinity in coastal aquifers affected by seawater intrusion. A combination of numerical modeling, staged chemical etching, and salinity calibration experiments was used to evaluate sensor performance. The key conclusions are as follows:

(1) A three-layer fiber waveguide model was established to simulate the effect of cladding etching on Bragg wavelength shifts. Numerical results confirmed that reducing the cladding diameter enhances evanescent field sensitivity, significantly improving salinity response. A clear linear relationship between Bragg wavelength shift and salinity was observed within the 0-6% salinity range.

(2) A staged etching process using high and low concentrations of hydrofluoric acid was employed to optimize both the etching efficiency and surface smoothness. This approach minimized surface defects, reduced stress-induced wavelength drift, and ensured stable sensor performance.

(3) Experimental results demonstrated that the EFBG sensor with a cladding diameter of 14.82 μm achieved a salinity sensitivity of 29.432 pm/%, with excellent linearity between Bragg wavelength shift and salinity. This high sensitivity, combined with the sensor's compact size, corrosion resistance, and real-time monitoring capability, makes it well-suited for long-term in-situ groundwater salinity monitoring in coastal areas.

Overall, the proposed EFBG sensor offers a practical and effective solution for groundwater salinity monitoring, contributing to improved seawater intrusion early warning and the protection of coastal infrastructure and water resources.

ACKNOWLEDGMENTS

This research was financially supported by the National Natural Science Foundation of China, NSFC (Grant Nos. 42177135, 42030701, 423B2704).

REFERENCES

[1] N. Kazakis, A. Pavlou, G. Vargemezis, K. S. Voudouris, G. Soulios, F. Pliakas, and G. Tsokas, Seawater intrusion mapping using electrical resistivity tomography and hydrochemical data: An application in the coastal area of eastern Thermaikos Gulf, Greece, Science of the Total Environment, vol. 543, pp. 373–387, 2016.

[2] L. Shi and J. J. Jiao, *Seawater intrusion and coastal aquifer management in China: A review*, Environmental Earth Sciences, vol. 72, pp. 2811–2819, 2014.

[3] S. Fadaie, M. Mehravar, D. J. Webb, and W. Zhang, *Nearshore contamination monitoring in sandy soils using polymer optical fibre Bragg grating sensing systems*, Sensors, vol. 22, pp. 1–19, 2022.

[4] J. Safarov, F. Millero, R. Feistel, A. Heintz, and E. Hassel, *Thermodynamic properties of standard seawater*, Ocean Science, vol. 6, pp. 689–722, 2009.

[5] I. Astin and Y. Feng, *Technical Note: Remote sensing of sea surface salinity using the propagation of low-frequency navigation signals*, Ocean Science, vol. 11, pp. 695–698, 2015.

[6] C. Woody, E. Shih, J. Miller, T. Royer, L. P. Atkinson, and R. S. Moody, *Measurements of salinity in the coastal ocean: A review of requirements and technologies*, Marine Technology Society Journal, vol. 34, no. 2, pp. 26–33, 2000.

[7] P. Grosso, M. Le Menn, J. L. De Bougrenet De La Tocnaye, Z. Y. Wu, and D. Malardé, *Practical versus absolute salinity measurements: New advances in high performance seawater salinity sensors*, Deep-Sea Research Part I: Oceanographic Research Papers, vol. 57, pp. 151–156, 2010.

[8] N. Vinogradova, T. Lee, J. Boutin, K. Drushka, S. Fournier, R. Sabia, D. Stammer, E. Bayler, N. Reul, A. Gordon, O. Melnichenko, L. Li, E. Hackert, M. Martin, N. Kolodziejczyk, A. Hasson, S. Brown, S. Misra, and E. Lindstrom, *Satellite salinity observing system: Recent discoveries and the way forward*, Frontiers in Marine Science, vol. 6, pp. 1–23, 2019.

[9] C. Gabarró, J. Font, A. Camps, M. Vall-llossera, and A. Julià, *A new empirical model of sea surface microwave emissivity for salinity remote sensing*, Geophysical Research Letters, vol. 31, pp. 1–5, 2004.

[10] B. Shi, D. Zhang, H. Zhu, C. Zhang, K. Gu, H. Sang, H. Han, M. Sun, and J. Liu, *DFOS applications to geo-engineering monitoring*, Photonic Sensors, vol. 11, pp. 158–186, 2021.

[11] J. Cong, X. Zhang, K. Chen, and J. Xu, *Fiber optic Bragg grating sensor based on hydrogels for measuring salinity*, Sensors and Actuators B: Chemical, vol. 87, pp. 487–490, 2002.

[12] P. Lu, L. Men, and Q. Chen, *Tuning the sensing responses of polymer-coated fiber Bragg gratings*, Journal of Applied Physics, vol. 104, 2008.

[13] K. Schroeder, W. Ecke, R. Mueller, R. Willsch, and A. Andreev, *A fibre Bragg grating refractometer*, Measurement Science and Technology, vol. 12, pp. 757–764, 2001.

[14] D. A. Pereira, *Fiber Bragg grating sensing system for simultaneous measurement of salinity and temperature*, Optical Engineering, vol. 43, p. 299, 2004.

[15] K. O. Hill and G. Meltz, *Fiber Bragg grating technology fundamentals and overview*, Journal of Lightwave Technology, vol. 15, pp. 1263–1276, 1997.

[16] J. Yang, H. Lee, and H. Sohn, *An optical fiber guided ultrasonic excitation and sensing system for online monitoring of nuclear power plants*, AIP Conference Proceedings, vol. 1430, pp. 1640–1647, 2012.

[17] A. N. Chryssis, S. M. Lee, S. B. Lee, S. S. Saini, and M. Dagenais, *High sensitivity evanescent field fiber Bragg grating sensor*, IEEE Photonics Technology Letters, vol. 17, pp. 1253–1255, 2005.

[18] M. Y. Sun, H. T. Jiang, B. Shi, G. Y. Zhou, H. I. Inyang, and C. X. Feng, *Development of FBG salinity sensor coated with lamellar polyimide and experimental study on salinity measurement of gravel aquifer*, Measurement, vol. 140, pp. 526–537, 2019.

[19] M. Monerie, *Propagation in doubly clad single-mode fibers*, IEEE Journal of Quantum Electronics, vol. 18, pp. 535–542, 1982.